DOI: 10.1002/ ((please add manuscript number))
Full Paper

Cavity Enhanced Organic Photodiodes with Charge Collection Narrowing

Aren Yazmaciyan, Paul Meredith, and Ardalan Armin**

A. Yazmaciyan
School of Mathematics and Physics
The University of Queensland
Brisbane 4072, Australia
Prof. P. Meredith, Dr. A. Armin
Department of Physics
Swansea University
Singleton Park, Swansea SA2 8PP, Wales, UK
E-mail: ardalan.armin@swansea.ac.uk; paul.meredith@swansea.ac.uk

Organic photodetectors, charge collection narrowing, charge transport, bulk heterojunctions, optical cavities

Colour discrimination in photodetection is conventionally achieved using broadband-absorbing inorganic semiconductors with passive optical filters. Organic semiconductors have shown promise to deliver narrowband spectral responses due to their tunable optical properties. While achieving narrow-absorbing organic semiconductors is an ongoing endeavour in the synthetic chemistry community, charge collection narrowing has been introduced as a 'material-agnostic' technique to realize narrowband spectral responses using broadband absorbers such as blends of organic semiconductors, inorganic nanocrystals and perovskites in a photodiode architecture. Charge collection narrowing in organic semiconductors demands photo-active junction thicknesses on the order of few microns causing fabrication difficulties and limitations in device metrics such as frequency bandwidth. In this work we show that electrical inversion can result in charge collection narrowing in organic photodiodes with active layer thicknesses on the order of 100s of nanometers and hence much easier to achieve *via* high throughput solution processing techniques. Additionally, we show that an indium tin oxide/gold electrode with modified work function acts as a cavity mirror further narrowing the spectral response

and at the same time delivering an extremely selective cathode suppressing the dark current dramatically. Nearly voltage independent detectivities of 10^{13} Jones are achieved with an active sensing area of 0.2 cm^2.

1. Introduction

Photodetection has become an essential component of everyday life and is deployed in a wide range of applications, including, but not limited to, colour sensing, visible light digital cameras, and machine vision.[1-5] Photodiodes are the most commonly used photodetecting optoelectronic device platform and can be spectrally categorised as either broadband or narrowband depending on the spectral bandwidth of the responsivity. Broadband photodiodes are generally favoured in multi-colour or broadband sensing since they have larger spectral bandwidths.[6] Conversely, narrowband or colour sensitive photodiodes are predominantly required in image sensors, medical sensing, intelligent surveillance, autonomous vehicles, and visible light communication[7] where only a restricted spectral range is the focus of detection.[4] The conventional way to realize a narrowband photodetector is to use a broadband photosensitive element optically coupled through passive bandpass filters.[8] This is the dominant technology in digital cameras and other image sensors. While this method delivers sufficient colour selectivity for everyday digital photography, it is not suited to more advanced applications such as machine vision, which demand detailed colour discrimination at the hardware level and not merely processed or enhanced in software.[9] Input optical filters also preclude true illuminant independent colour discrimination and replication – again, a preferred requirement for artificial vision. Furthermore, the use of arrays of passive filters results in limitations in increasing the spatial resolution of image sensors.[4] The use of photodetector technologies, which are inherently sensitive to specific colour ranges (red-green-blue for example) is thus a means to overcome the need for passive filter arrays.

New generations of semiconductors such as organics, perovskites and inorganic nanocrystals with tailorable optical properties have been proposed as one solution to achieve wavelength sensitivity since the spectral nature of their optical absorptions can be manipulated and indeed designed by molecular-level engineering and/or altering quantum confinement level.[10-14] However, achieving adequate responsivities in a particular narrow colour window whilst ensuring darkness outside that window has proven challenging, if not impossible. Device-based architectural approaches utilizing these semiconductors are also emerging by employing electro-optical control.[15] Charge Collection Narrowing (CCN) is one such favoured and promising example where the narrowband response is delivered by controlling the photo-generated charge collection efficiency in so-called thick junctions (of order 1 μm or greater).[16] Such thick junctions with limited charge transport exhibit very different electro-optical properties to conventional photodiodes.[17-19] The technique was introduced as a "material-agnostic" strategy by Armin *et al*.,[16] and it has been realised in other material systems including solution processed lead halide perovskites,[20-22] perovskite single crystals,[23, 24] organic-inorganic composites,[25, 26] quantum dots,[27] and molecular nano-ribbons.[28] However, the requirement for thick junctions when CCN is employed in organic semiconductor photodiodes is a considerable fabrication limitation. Whilst the creation of relatively thin junctions (~ 100s of nm) is favoured by solution processing techniques, very thin (<100 nm) and very thick (on the order of several microns) junctions are much more difficult to achieve especially using high throughput deposition methods suited to organic semiconductors. Moreover, extremely thick photodiodes have limited frequency bandwidths due to the long carrier transit times.[23] Hence, achieving CCN in thinner junctions would dramatically enhance the potential utility of the approach and extend the available range of suitable organic semiconductors. Another architectural electro-optical approach is the use of micro-cavities in donor/acceptor organic semiconductor blends. This strategy has recently been used to amplify

direct photoexcitation of charge transfer (CT) states,[29, 30] which can contribute in charge generation if they absorb light efficiently. An interesting and unexplored question is whether the CCN and micro-cavity approaches can be combined to deliver enhanced performance in organic semiconductor photodiodes. In this regard, the challenge is the need for very thick junctions which in the presence of a micro-cavity exhibit several resonance peaks due to the smaller mode separation when the cavity length is large.

In this communication, narrowband organic semiconductor photodetectors utilising the CCN effect are presented with junction thicknesses much smaller than previously reported.[16] It is shown that electrical inversion of charge transport can induce even more unbalanced electron and hole transit times resulting in the CCN effect in junctions with thicknesses less than a micron. The micro-cavity concept is applied to these CCN photodiodes and the thinner junctions mean that the mode separations are large enough to avoid multimode spectral resonances. As a result, additional spectral narrowing is achieved. Furthermore, an indium tin oxide (ITO)/gold (Au)/polyethylenimine (PEIE) electrode (acting as a mirror in the cavity) is introduced which also performs as an ultra-selective cathode lowering the dark current and the noise. Specific detectivities of 10^{13} Jones are achieved.

2. Results

In the context of organic optoelectronics, a ‘thin film’ device such as a solar cell, photodetector or light emitting diode has an active layer thickness on the order of a fraction of a micron, and typically hundreds of nanometers. In the presence of a semi-transparent electrode these devices act as low finesse cavities,[31, 32] where the optical absorption profile and charge carrier transport are strongly coupled.[17, 33] This results in electro-optical physics more complex than other types of so-called thin film devices such as those made of amorphous silicon and compound semiconductors (CdTe solar cells as an example), which have considerably thicker junctions with electron/hole pair diffusion lengths of order 10s of microns. In addition, organic

semiconductors exhibit large absorption coefficients (typically $\alpha \approx 10^5$ cm^{-1}) when the photon energy is greater than the optical gap. A broad absorption tail is also observed arising from energetic disorder and natural broadening of the spin singlet excitations (excitons). As such, the absorption gradually vanishes near the absorption onset over a spectral bandwidth of 50-100 nm rather than being a distinct step-function. Furthermore, direct electronic coupling of the CT states to the ground state provides additional broadening to the tail absorption in donor: acceptor blends. For the model organic semiconductor blend system PCDTBT:PC70BM (poly[*N*-9″-heptadecanyl-2,7-carbazole-*alt*-5,5-(4′,7′-di-2-thienyl-2′,1′,3′-benzothiadiazole)]:phenyl-C70-butyric acid methyl ester), with molecular structures as depicted in **Figure 1**a, the absorption spectrum is shown in Figure 1b. The aforementioned broad absorption tail in the spectrum is clearly observed. Figures 1(c-e) show typical external quantum efficiency (EQE) spectra for sandwich-type photodiodes with the simple architecture (ITO/poly(3,4-ethylenedioxythiophene): poly(styrene sulfonate) (PEDOT:PSS)/ PCDTBT:PC70BM/samarium (Sm)/aluminium (Al)) and three different active layer thicknesses, 100 nm, 700 nm, and 2600 nm. The photon absorption profiles were simulated using the transfer matrix method for blue (400 nm) and red (600 nm) photons and are shown as insets. If the junction thickness *d*, is smaller than the inverse of the absorption coefficient (i.e., $d < \alpha^{-1}$), the photon absorption profile for incident wavelengths with low and high absorption coefficient (red and blue respectively) are more or less distributed in the bulk (Figure 1c inset). This device is, therefore considered as "optically thin". When $d \gg \alpha^{-1}$, blue/green photons are mostly absorbed near the transparent (light input-coupling) electrode with a Beer-Lambert-like profile, while red photons from the tail of the absorption can penetrate into the volume resulting in back reflection from the counter electrode and thus cavity interference. This is the case for devices with junction thicknesses of 700 nm and 2600 nm, which should be considered "optically thick".

It is now important to recognise the differences in charge carrier generation and subsequent transport in these three devices. Whilst the 700 nm-thick junction is optically thick with blue/green photons absorbed near the anode, the charge carrier transport can still be efficient for both blue and red photons – holes in the PCDTBT:PC70BM blend are 100 times slower than electrons,[34] but they are generated closer to their respective collection electrode. As such, while the 700 nm device is optically thick, in terms of charge carrier transport both 100 nm and 700 nm junctions are "electrically thin" with the EQE spectra being broadband. The term 'electrically thin active layer' implies that the minority carriers' (near the ITO electrode) transit time ($t_{\mathrm{tr}} = d^2/V\mu_m$, where d is the active layer thickness with voltage V across it, and μ_m the minority carriers mobility) is shorter than their lifetime τ, and therefore the drift distance of the minority carriers is larger than the active layer thickness. This leads to efficient charge collection. This scenario changes, when the junction thickness increases (here, up to 2600 nm). Electrons derived from blue-photons are generated near the anode (ITO electrode in conventional architecture) and as such, much further away from the cathode. These electrons must travel across the active layer thickness, and hence have a lower extraction rate (longer transit time so that $t_{\mathrm{tr}|e} > \tau_e$). This also results in higher electron density (minority carriers) near the ITO/PEDOT:PSS contact lowering the lifetime of the majority carriers, holes, so that $t_{\mathrm{tr}|h} > \tau_h$. This makes such optically thick devices also "electrically thick" giving rise to the charge carrier recombination and a poor charge collection of those carriers generated near the ITO contact (blue-generated charges). At wavelengths near the absorption onset, where the absorption coefficient is small ($\alpha d \ll 1$), resultant charge carriers are extracted efficiently creating the CCN spectral peak in the EQE. This is the basic physical principle of charge collection narrowing (CCN) although one must acknowledge that a complete mechanistic understanding of the CCN process is yet to emerge. Since the electrons are faster in PCDTBT:PC70BM and actually most other donor: acceptor blends, to obtain CCN in organic

semiconductor photodiodes one generally requires ultra-thick junctions on the order of several microns to deliver this narrowband response via unbalanced transit times of electrons and holes.

The next question to address is whether the 700 nm-thick junction can be converted to an electrically thick device (thus yielding the CCN effect) by electrical inversion of the structure such that the transparent electrode is electron extracting (cathode) (**Figure 2**a, b). In the case of PCDTBT:PC70BM, since the holes have lower mobility (on the order of 10^{-5} $cm^2V^{-1}s^{-1}$) than electrons (~ 10^{-3} $cm^2V^{-1}s^{-1}$),[34] electrical inversion will result in increased hole transit times and higher hole (now acting as minority carriers) near the transparent cathode. This results in recombination of charges generated near the cathode and thereby CCN. The EQE spectra of conventional and electrically inverted PCDTBT:PC70BM (700 nm) photodiodes are shown in Figure 2c with a CCN peak clearly observed thus proving this principle.

By using the electrically inverted architecture which delivers a CCN effect with sub-micron junction thickness and introducing a partially reflecting cathode, the quality factor of the "cavity" could be increased to facilitate further spectral narrowing. Schematics of the device structures are shown in **Figure 3**. The 20 nm gold layer was modified with PEIE (as described in the experimental section), and as will be evident later, this electrode operates as an extremely selective electron extracting contact. A MoO_x/Ag electrode was thermally evaporated onto the top of the device as the anode. Going forward, the devices with the Au layer are referred as "high-Q cavity" and the ones without the Au layer as "low-Q cavity" – although it must be said that in conventional optics both would be considered very low-Q.

The next step toward optimization of the CCN response was to overlap the EQE peak in the absorption edge of the material system with the cavity mode of the high-Q devices. This required fine tuning of the active layer thickness to vary the position of the cavity mode (see Supporting Information **Figure S1**). It was found that in devices with an active layer thickness

of 850 nm, one of the cavity overtone modes overlapped with the CCN peak causing further narrowing as shown in **Figure 4**a. The full width at half maximum (FWHM) of the low-Q photodiode is approximately 100 nm, which is lowered to 50 nm in the high-Q photodiode. The positions of the cavity modes were determined from the transmission spectra of the devices (shown as dashed lines Figure 4a). The position of one of the cavity modes matches with the CCN peak in the low-Q device (shown as grey open circles in Figure 4b) and another cavity mode overlaps with the charge transfer (CT) states enhancing their absorption. The CCN peak and the CT state responses in the high-Q device were both considerably narrowed and could also be fitted with Lorentzian functions confirming them to be cavity-enhanced.

3. Performance Metrics of the Photodiodes

Aside from photo-responsivity, $R(\lambda)$ (given by the EQE), perhaps the most important figure of merit for a photodetector is its noise current. The noise current (i_{noise}) is the root-mean-square of the dark shot noise (proportional to the root-square of the dark current), thermal Johnson-Nyquist noise (related to the shunt resistance) and the less-understood component of flicker noise with power spectrum, $i_{1/f}^2(\omega)$.[21][35] The noise current is thus

$$\langle i_n^2(\omega)\rangle = \left[2q\langle i_d\rangle + \frac{4k_BT}{R_{\text{shunt}}} + i_{1/f}^2(\omega)\right]\Delta f \tag{1}$$

The minimum detectable power (NEP) is the incident light power at which the signal-to-noise ratio (SNR) is unity at an electrical bandwidth, Δf. The NEP is given by

$$\text{NEP} = \frac{i_n}{R}. \tag{2}$$

The inverse of the NEP normalised to the device area and the electrical bandwidth yields the specific detectivity (D^*) which is often taken as a device metric appropriate for comparing different types of photodetectors with different device areas measured at different electrical bandwidths

$$D^* = \frac{\sqrt{A\Delta f}}{\text{NEP}}. \tag{3}$$

While the actual and carefully measured noise was relied upon in this study, it is also useful to correlate this with the calculated noise components for completeness. The dark current density as a function of reverse bias voltage for the low- and high-Q devices are shown in **Figure 5**a. While the junction thickness remains the same in these two types of device, there is orders of magnitude difference in the dark current. The suppressed dark current in the high-Q device is assigned to the ITO/Au/PEIE cathode, which performs as an extremely selective electrode for collecting electrons. The measured noise current, shot and thermal components are shown in Figure 5(b, c) for low- and high-Q photodiodes. The noise current of the high-Q device with the ITO/Au/PEIE electrode is at least two orders of magnitude smaller than the low-Q device with the ITO/PEIE electrode. It can also be observed that the measured noise (obtained from the plateau of the noise spectral density – see Supporting Information) is at least an order of magnitude larger than the calculated noise from Equation 1. This again shows the importance of a full noise measurement in order to avoid an underestimation of the noise current, and thus an overestimation of D^*. The noise was measured by applying a Fast Fourier Transform (FFT) on the current as a function of time at different electrical bandwidths (set by the measurement time) and the results shown in Figure 5(b, c) are the noise currents normalised to these bandwidths.

The D^* and NEP can now be calculated for the photodiodes from the measured noise presented in Figure 5 and Equations 2 and 3. **Figure 6** shows (a) the NEP and (b) the D^* for low- and high-Q photodiodes, respectively. A state-of-the-art NEP of 30 fW/√Hz is achieved with the high-Q photodiodes corresponding to a specific detectivity of 10^{13} Jones with device area of 0.2 cm^2. Such metrics can also be obtained with small-area broadband inorganic semiconductors photodiodes. However, in this case the extremely low NEP is achieved together with a narrowband response and a relatively large device area. It should be noted that this NEP is calculated from Equation 2 from the measured noise and not directly measured via

ultra-low power spectral responsivity measurement we recently proposed.[36] Such an extrapolation may be acceptable for detectors without photo-conductive gain (as is the case here) but is not always valid especially in the case of trap-engineered devices.

Finally, the -3dB cut-off frequency bandwidths of the photodiodes were measured. This parameter is dependent upon the RC-time of the circuit and the charge carrier transit time (t_{tr}). Predominantly, it is the slower carrier transit time that limits the bandwidth in disordered systems such as organic semiconductors. The -3dB bandwidth is given by[37]

$$\frac{1}{f_{-3\mathrm{dB}}^2} = \frac{1}{f_t^2} + \frac{1}{f_{\mathrm{RC}}^2} \tag{4}$$

where $f_t = \frac{3.5}{2\pi t_{\mathrm{tr}}}$ and $f_{RC} = \frac{1}{2\pi RC}$ are the transit time-limited and RC-limited bandwidths, respectively with t_{tr} being the transit time of the slower carriers. The bandwidths were quantified using a fast LED at a wavelength of 650 nm and excitation power of ~ 0.1 mW. The LED was driven with a Vector Network Analyser. The coherent power transmission from the LED to the photodetector (connected to the other port of the analyser) was recorded in units of dBm (power). This is the off-diagonal element of the scattering matrix measured by the network analyser. A -3dB frequency bandwidth of ~ 100 kHz was determined. The RC limit of the photodetector was found to be 2 MHz (see Supporting Information). Therefore, the response speed could not be further increased by reducing the device area and it is intrinsically limited by the charge carrier transit time.

4. Conclusion

Organic photodiodes (OPDs) with charge collection narrowing (CCN) and utilising a model broadband organic semiconductor blend system (PCDTBT:PC70BM) have been demonstrated with junction thicknesses less than a micron – much thinner than previously reported. This has been achieved *via* electrical inversion of the device architecture that induces further imbalance in electron and hole transit times and thereby delivers CCN. The use of a micro-cavity further

narrowed the spectral response and also enabled the charge transfer states to contribute to the photoresponse in the tail of the CCN peak. It was also found that ITO/Au/PEIE is an extremely selective cathode. This electrode not only acted as a mirror for increasing the quality factor of the cavity but also decreased the dark and noise current. A noise equivalent power of nearly 30 fW (at unity bandwidth) and a virtually voltage independent specific detectivity of 10^{13} Jones were achieved. We believe this to be a generic methodology for achieving enhanced narrowband spectral responses in OPDs whilst reducing limitations imposed by thick junctions.

5. Experimental Section

Device fabrication: Organic photodetectors were fabricated on glass substrates that were already coated with pre-patterned indium tin oxide (ITO) layer (Xinyan: 15 Ω sq^{-1}) in a class 1000 cleanroom. First, the substrates were washed in Alconox solution at 80 °C for 10 min, that is, a detergent bath which was then followed by sonication in deionized water, acetone and isopropanol, respectively, each at 40 °C for 10 min. After blow-drying the substrates with a nitrogen gun, a PEDOT:PSS (Heraeus Clevios P VP AI 4083) layer was spun cast onto the substrates at 5000 rpm for 30 s which gave a 30±5 nm-thick hole transporting layer for conventional OPDs. The PEDOT:PSS coated substrates were baked at 165 °C for 10 min. A PEIE solution (0.05 wt% in 2-methoxyethanol) was spun cast at 5000 rpm for 60 s, and annealed subsequently at 100 °C for 10 min in ambient air to form an electron transporting layer for the electrically inverted OPDs. The substrates were then transferred into a nitrogen atmosphere glove box (O_2 <1 ppm, H_2O <1 ppm) for the deposition of the respective photoactive layers. PC70BM (American Dye Source) was dissolved in anhydrous 1,2-dichlorobenzene (DCB) at 70 °C and left on a magnetic stirrer overnight to make a 28 mg/ml solution. The PC70BM solution was cooled down to room temperature and filtered with a 0.2µ PTFE filter before adding 1 ml of it to 7 mg PCDTBT ($\bar{M}_w$ = 122.2 kDa, PDI = 5.4, SJPC

Canada). The blend solution (35 mg/ml 1:4 by weight) was then heated to 160 °C and left stirring for an hour until the PCDTBT dissolved completely. Before dispensing the PCDTBT:PC70BM solution onto the cleaned substrates, it was cooled down to room temperature slowly to control its viscosity (according to the citation[38]) by switching off the heating feature of the magnetic stirrer, while still stirring on the hot plate. For the conventional photodetectors, the 2600 nm-thick PCDTBT:PC70BM film was obtained by spin coating of a 50 mg/ml blend solution at 400 rpm for 30 min. The 700 nm-thick film was deposited by spin coating of a 35 mg/ml blend solution at 500 rpm for 15 min, and 100 nm-thick film by spin coating of a 22.5 mg/ml blend solution at 1200 rpm. After the deposition of photoactive layers, the substrates were annealed at 50 °C for 5 min to facilitate additional residue solvent evaporation. Finally, the substrates were transferred into the thermal evaporation chamber in the glove box for the deposition of respective metal contacts (MoO_x/Ag as the anode for inverted, Sm/Al as cathode for conventional devices) under a 10^{-6} mbar vacuum with a mask to realize a device area of 0.2 cm^2.

Device characterization: IV curves and current-time traces were recorded using an Agilent 1500B parametric semiconductor analyser. Triax cables and a Faraday cage were used to minimise pick-up noise. The EQE spectra were measured using a PV Measurements Inc. QEX7 system at a chopping frequency of 120 Hz and a bandwidth of 1 Hz. The noise currents were determined by integrating the Fast Fourier Transform (FFT) of the dark currents measured with electrical bandwidths of 0.01 and 0.1 Hz where the noise floor was reached. Film thicknesses were determined using a surface profilometer (Veeco Dektak 150).

Transfer matrix simulations: A computational code based on transfer matrix method developed by van de Lagemaat et al. from the National Renewable Energy Laboratory (NREL) was used to simulate the optical field distribution and the absorption profiles.[31]

Supporting Information
Supporting Information is available from the Wiley Online Library or from the author.

Acknowledgements
A.Y. was supported by a University of Queensland International Postgraduate Research Scholarship. P.M. is a Sêr Cymru Research Chair, and was formally an Australian Research Council Discovery Outstanding Research Award Fellow. A.A. is a Rising Star Sêr Cymru Fellow. This program was supported by the Australian Government through the Australian Renewable Energy Agency (ARENA) Australian Centre for Advanced Photovoltaics. The work was performed in part at the Queensland node of the Australian National Fabrication Facility (ANFF): a company established under the National Collaborative Research Infrastructure Strategy to provide nano and micro fabrication facilities for Australia's researchers.

Received: ((will be filled in by the editorial staff))
Revised: ((will be filled in by the editorial staff))
Published online: ((will be filled in by the editorial staff))

The table of contents entry should be 50–60 words long: Narrowband organic photodiodes are reported which exhibit cavity enhanced charge collection narrowing in junctions thinner than previously realized. These photodetectors possess a state-of-the-art noise equivalent power of nearly 30 fW (at unity bandwidth) and a virtually voltage independent specific detectivity of 10^{13} Jones. This is a generic strategy to create narrowband spectral responses in broadband absorbing organic semiconductors.

Keyword Organic photodetectors, charge collection narrowing, charge transport, bulk heterojunctions, optical cavities

Aren Yazmaciyan, Paul Meredith*, and Ardalan Armin*

Cavity Enhanced Organic Photodiodes with Charge Collection Narrowing

ToC figure ((Please choose one size: 55 mm broad × 50 mm high **or** 110 mm broad × 20 mm high. Please do not use any other dimensions))

References

[1] G. Konstantatos, E. H. Sargent, *Nat Nanotechnol* **2010**, *5*, 391.
[2] K.-J. Baeg, M. Binda, D. Natali, M. Caironi, Y.-Y. Noh, *Advanced Materials* **2013**, *25*, 4267.
[3] K. H. Lee, D. S. Leem, J. S. Castrucci, K. B. Park, X. Bulliard, K. S. Kim, Y. W. Jin, S. Lee, T. P. Bender, S. Y. Park, *ACS Appl Mater Interfaces* **2013**, *5*, 13089.
[4] R. D. Jansen‐van Vuuren, A. Armin, A. K. Pandey, P. L. Burn, P. Meredith, *Advanced Materials* **2016**, *28*, 4766.
[5] F. P. G. de Arquer, A. Armin, P. Meredith, E. H. Sargent, *Nature Reviews Materials* **2017**, *2*, 16100.
[6] R. Saran, R. J. Curry, *Nat Photonics* **2016**, *10*, 81.
[7] T. Yamazato, I. Takai, H. Okada, T. Fujii, T. Yendo, S. Arai, M. Andoh, T. Harada, K. Yasutomi, K. Kagawa, S. Kawahito, *IEEE Communications Magazine* **2014**, *52*, 88.
[8] Y. Horie, S. Han, J.-Y. Lee, J. Kim, Y. Kim, A. Arbabi, C. Shin, L. Shi, E. Arbabi, S. M. Kamali, *Nano letters* **2017**, *17*, 3159.
[9] T. Suzuki, "Challenges of image-sensor development", presented at *2010 IEEE International Solid-State Circuits Conference - (ISSCC)*, 7-11 Feb. 2010, 2010.
[10] S. A. McDonald, G. Konstantatos, S. Zhang, P. W. Cyr, E. J. Klem, L. Levina, E. H. Sargent, *Nat Mater* **2005**, *4*, 138.
[11] G. Konstantatos, I. Howard, A. Fischer, S. Hoogland, J. Clifford, E. Klem, L. Levina, E. H. Sargent, *Nature* **2006**, *442*, 180.
[12] T. Rauch, M. Boberl, S. F. Tedde, J. Furst, M. V. Kovalenko, G. Hesser, U. Lemmer, W. Heiss, O. Hayden, *Nat Photon* **2009**, *3*, 332.
[13] L. Zhu, W. S. Wang, Z. G. Yao, X. Zhang, Y. Wang, *IEEE Transactions on Electron Devices* **2012**, *59*, 3583.
[14] D. M. Lyons, A. Armin, M. Stolterfoht, R. C. Nagiri, R. D. Jansen-van Vuuren, B. N. Pal, P. L. Burn, S.-C. Lo, P. Meredith, *Organic Electronics* **2014**, *15*, 2903.
[15] J. M. Lupton, R. Koeppe, J. G. Müller, J. Feldmann, U. Scherf, U. Lemmer, *Advanced Materials* **2003**, *15*, 1471.
[16] A. Armin, R. D. Jansen-van Vuuren, N. Kopidakis, P. L. Burn, P. Meredith, *Nat Commun* **2015**, *6*, 6343.
[17] J. G. Tait, U. W. Paetzold, D. Cheyns, M. Turbiez, P. Heremans, B. P. Rand, *ACS applied materials & interfaces* **2016**, *8*, 2211.
[18] W. Wang, F. Zhang, M. Du, L. Li, M. Zhang, K. Wang, Y. Wang, B. Hu, Y. Fang, J. Huang, *Nano Lett* **2017**, *17*, 1995.
[19] J. Miao, F. Zhang, M. Du, W. Wang, Y. Fang, *Phys Chem Chem Phys* **2017**, *19*, 14424.
[20] Q. Lin, A. Armin, P. L. Burn, P. Meredith, *Nature Photonics* **2015**, *9*, 687.
[21] M. I. Saidaminov, M. A. Haque, M. Savoie, A. L. Abdelhady, N. Cho, I. Dursun, U. Buttner, E. Alarousu, T. Wu, O. M. Bakr, *Advanced Materials* **2016**, *28*, 8144.
[22] L. L. Li, Y. H. Deng, C. X. Bao, Y. J. Fang, H. T. Wei, S. Tang, F. J. Zhang, J. S. Huang, *Advanced Optical Materials* **2017**, *5*, 1700672.
[23] Y. Fang, Q. Dong, Y. Shao, Y. Yuan, J. Huang, *Nature Photonics* **2015**, *9*, 679.
[24] H. S. Rao, W. G. Li, B. X. Chen, D. B. Kuang, C. Y. Su, *Advanced Materials* **2017**, *29*, 1602639.
[25] L. Shen, Y. Fang, H. Wei, Y. Yuan, J. Huang, *Advanced Materials* **2016**, *28*, 2043.
[26] M. R. Esopi, E. Zheng, X. Zhang, C. Cai, Q. Yu, *Physical Chemistry Chemical Physics* **2018**, *20*, 11273.

[27] K. Qiao, H. Deng, X. Yang, D. Dong, M. Li, L. Hu, H. Liu, H. Song, J. Tang, *Nanoscale* **2016**, *8*, 7137.
[28] Y. Zhong, T. J. Sisto, B. Zhang, K. Miyata, X.-Y. Zhu, M. L. Steigerwald, F. Ng, C. Nuckolls, *Journal of the American Chemical Society* **2017**, *139*, 5644.
[29] B. Siegmund, A. Mischok, J. Benduhn, O. Zeika, S. Ullbrich, F. Nehm, M. Böhm, D. Spoltore, H. Fröb, C. Körner, K. Leo, K. Vandewal, *Nature communications* **2017**, *8*, 15421.
[30] Z. Tang, Z. Ma, A. Sánchez‐Díaz, S. Ullbrich, Y. Liu, B. Siegmund, A. Mischok, K. Leo, M. Campoy‐Quiles, W. Li, K. Vandewal, *Advanced Materials* **2017**, *29*, 1702184.
[31] P. Peumans, A. Yakimov, S. R. Forrest, *Journal of Applied Physics* **2003**, *93*, 3693.
[32] A. Armin, Y. Zhang, P. L. Burn, P. Meredith, A. Pivrikas, *Nat Mater* **2013**, *12*, 593.
[33] A. Armin, A. Yazmaciyan, M. Hambsch, J. Li, P. L. Burn, P. Meredith, *ACS Photonics* **2015**, *2*, 1745.
[34] A. Armin, M. Velusamy, P. Wolfer, Y. Zhang, P. L. Burn, P. Meredith, A. Pivrikas, *Acs Photonics* **2014**, *1*, 173.
[35] S. Xiong, L. Li, F. Qin, L. Mao, B. Luo, Y. Jiang, Z. Li, J. Huang, Y. Zhou, *ACS Appl Mater Interfaces* **2017**, *9*, 9176.
[36] Y. Fang, A. Armin, P. Meredith, J. HUang, *Nature Photonics* **2018**.
[37] A. Armin, M. Hambsch, I. K. Kim, P. L. Burn, P. Meredith, E. B. Namdas, *Laser & Photonics Reviews* **2014**, *8*, 924.
[38] P. Wolfer, A. Armin, A. Pivrikas, M. Velusamy, P. L. Burn, P. Meredith, *Journal of Materials Chemistry C* **2014**, *2*, 71.

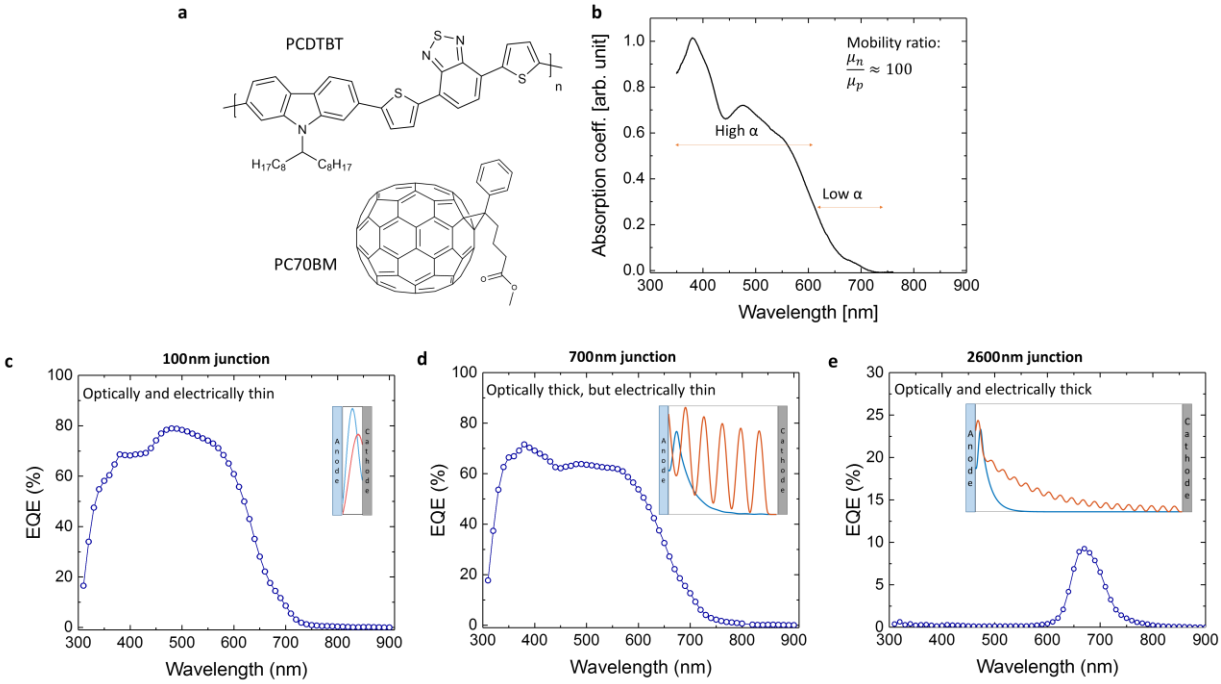

Figure 1. (**a**) Molecular structure of PCDTBT and PC70BM, used as a model system in this study. (**b**) Absorption coefficient of a PCDTBT:PC70BM (1:4 by weight) thin film. (**c-e**) External Quantum Efficiency (EQE) spectra of photodiode devices with the structure ITO/PEDOT:PSS/PCDTBT:PC70BM/Sm/Al and varying junction thicknesses as marked on the figures. The insets show the modelled photon absorption profile for blue (400 nm) and red (600 nm) photons obtained using a transfer matrix approach.

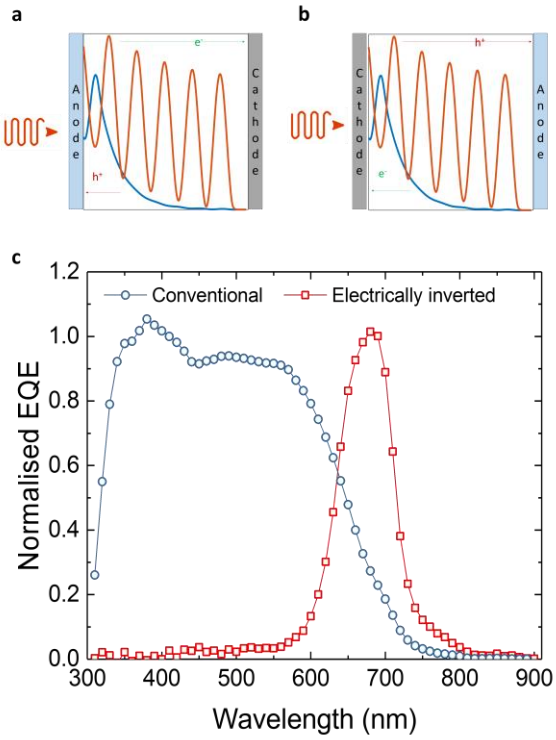

Figure 2. (**a**, **b**) Modelled absorbed photon profiles in 700 nm thick junctions with the charge carrier transport directions indicated. In the case of the electrically inverted device (**b**), the holes generated by blue photons are effectively further away from their extracting electrode (anode) resulting in charge collection narrowing. (**c**) The measured (normalised) EQE for a conventional and electrically inverted device confirming the modelling and noting the conventional device exhibits a broadband response and the inverted CCN-derived narrowband.

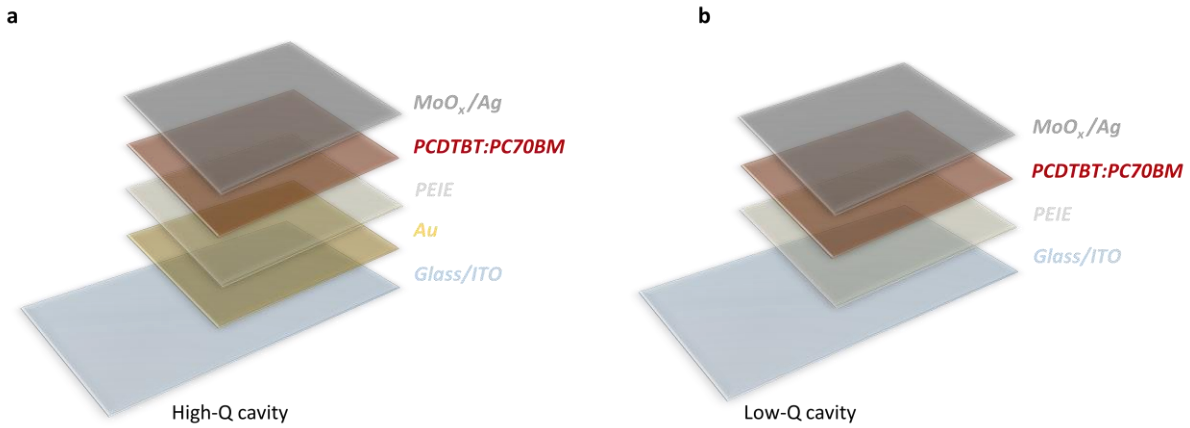

Figure 3. Introduction of a thin Au layer to improve the finesse of the cavity. Device architectures of high- (**a**) and low-Q (**b**) cavity electrically inverted OPDs. The 20 nm-thick Au layer was deposited thermally to amplify the resonances at certain wavelengths and over the CCN (and CT state) responsivity peaks.

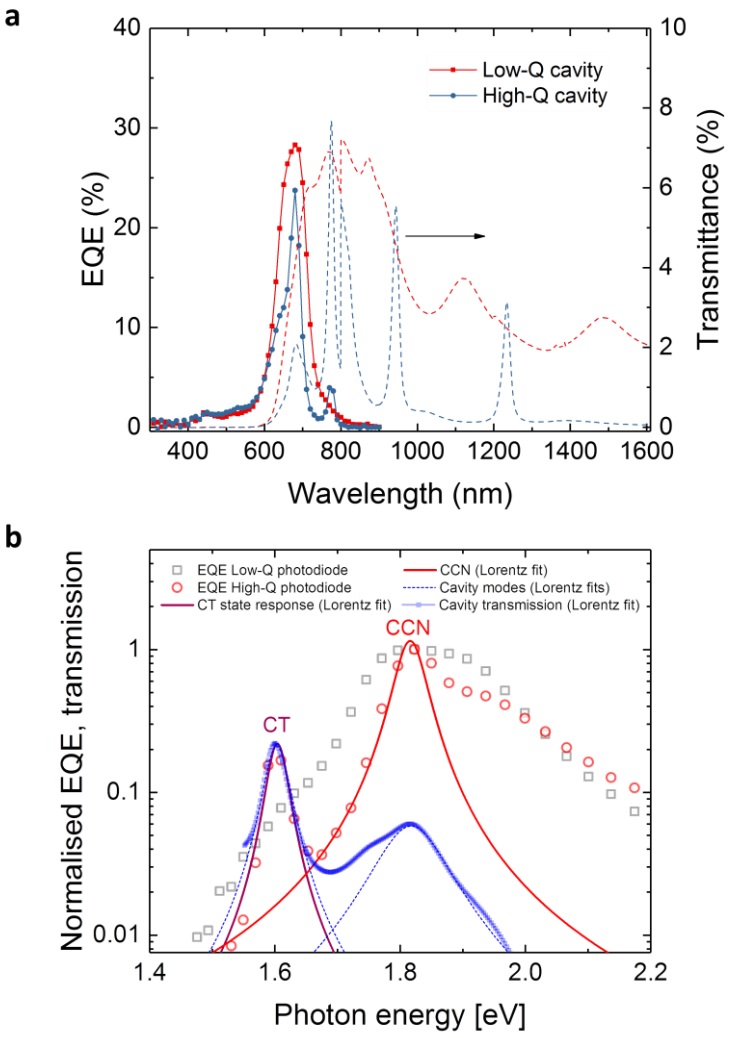

Figure 4. Performance comparison of high- and low-Q cavity OPDs. (**a**) EQE and transmission spectra of low- and high-Q PCDTBT:PC70BM electrically inverted organic photodiodes measured at -1V and 120 Hz. (**b**) Normalised EQE and transmission of the high-Q photodiode and the EQE spectrum of the low-Q photodiode. The cavity peaks from the transmission spectrum are fitted with Lorentzian functions. The corresponding cavity enhanced EQE peaks are also fitted with Lorentzian functions. The Q-factors of low- and high-Q devices are approximately 2.5 and 40 respectively [determined from the approximated mode width of the transmittance spectra shown in (a)].

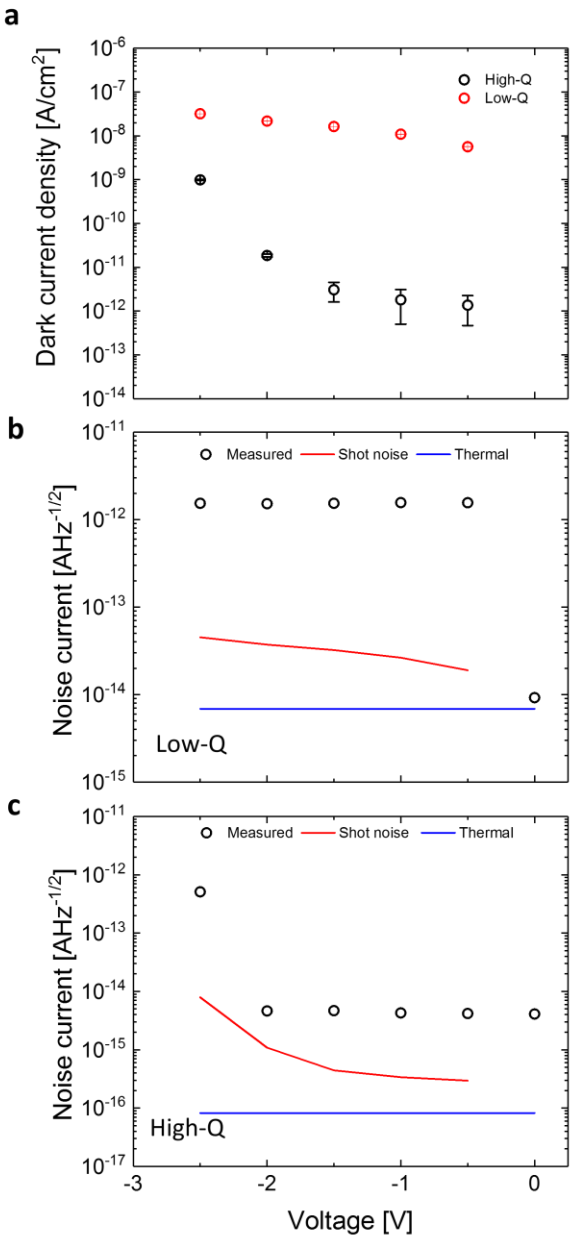

Figure 5. Dark and noise current measurements. (**a**) Dark current density as a function of applied voltage for low- and high-Q photodiodes. The error bars indicate standard deviations of the current from the time-averaged current. (**b**, **c**) Measured noise current from the Fast Fourier Transform (FFT) of high-resolution current-time measurements along with the calculated shot and thermal noise for low- and high-Q photodiodes.

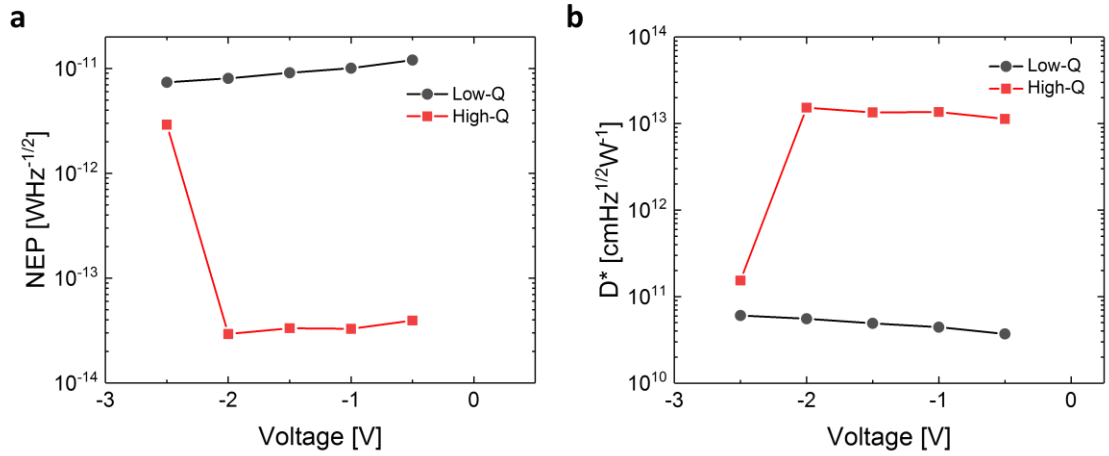

Figure 6. Noise equivalent power (NEP) and specific detectivity (D*). (**a**) NEP and (**b**) specific detectivity of low- and high-Q photodiodes. These metrics are more than two orders of magnitude superior in the case of the high-Q device using a selective ITO/Au/PEIE electrode. An NEP of order of fW/√Hz is achieved with the high-Q device and the D* is voltage independent out to -2 V.

Supporting Information

Cavity Enhanced Organic Photodiodes with Charge Collection Narrowing

Aren Yazmaciyan, Paul Meredith, and Ardalan Armin**

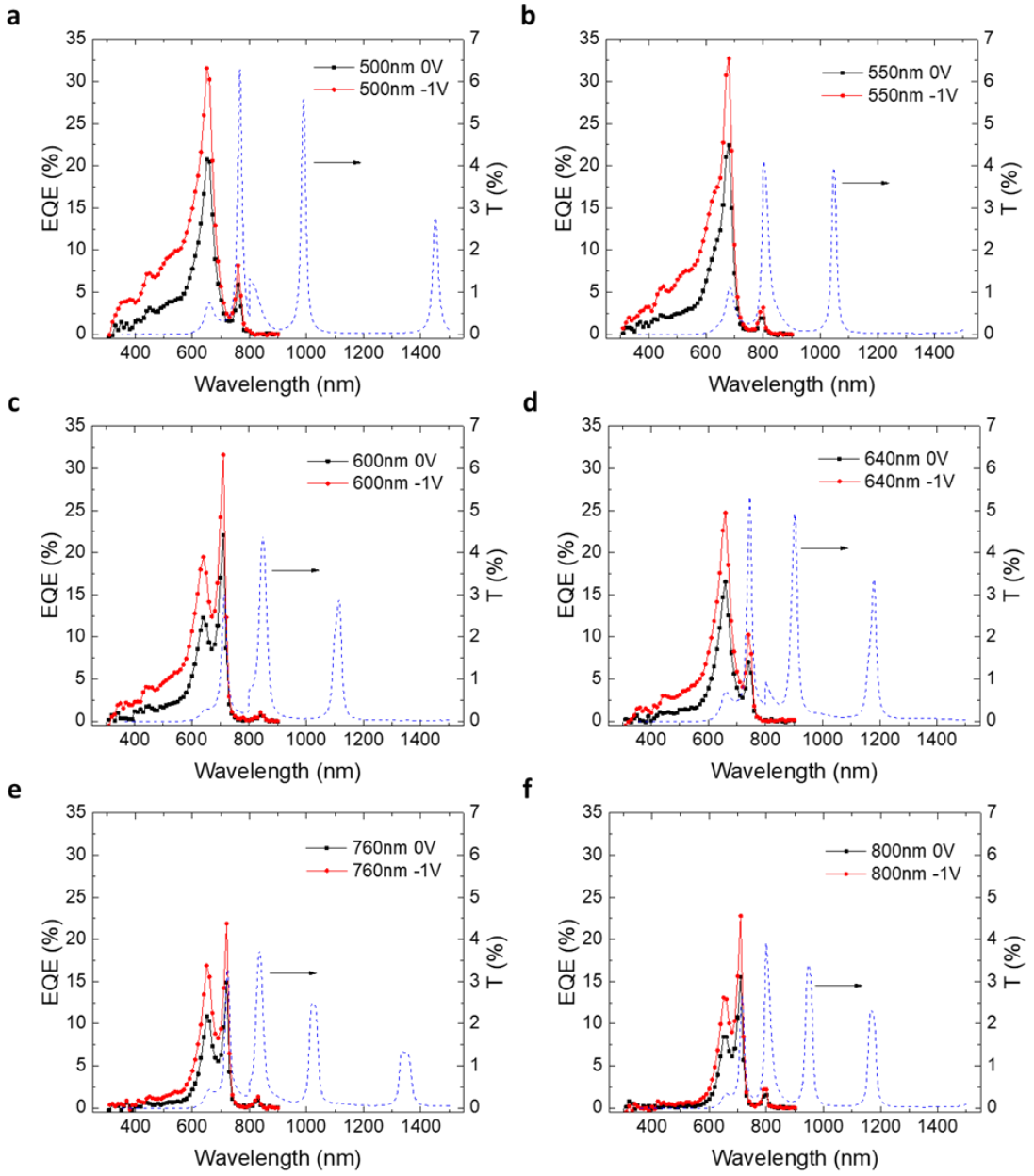

Figure S1 Effect of thickness on the spectral response of the high-Q OPDs. The dashed line is the transmission indicating the cavity mode and it is clear how tuning the junction thickness moves the cavity modes.

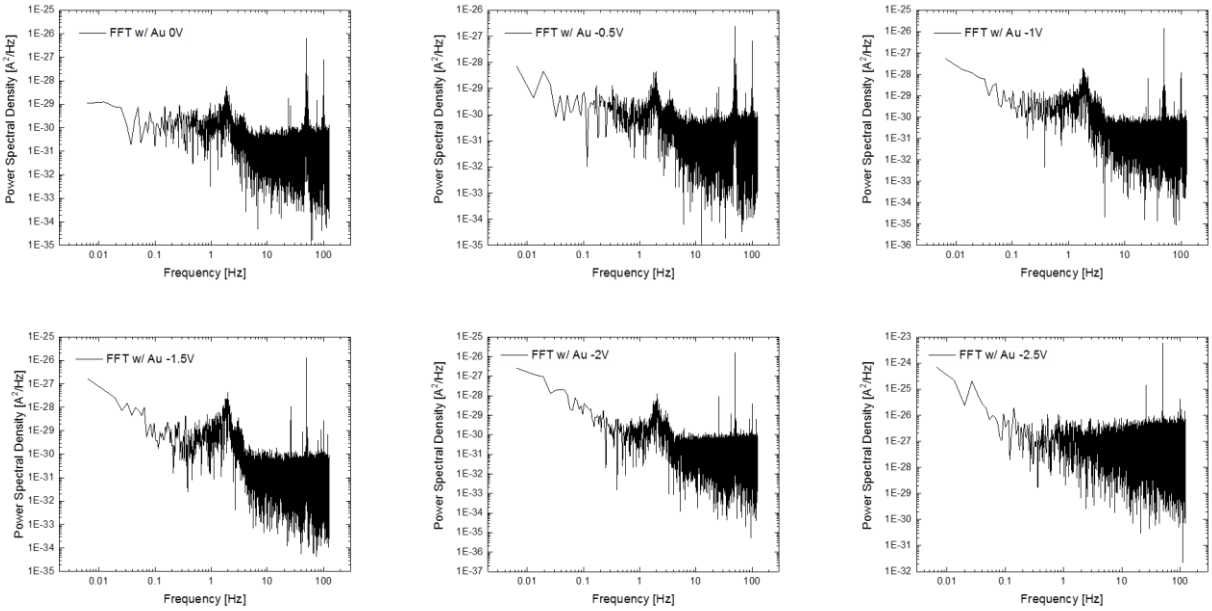

Figure S2 Noise spectral density of high-Q electrically inverted OPDs at various voltages measured at a bandwidth of 0.01 Hz (100 second time constant). These results were obtained by applying a fast Fourier transform on the current versus time measured up to 200s with intervals of 4 ms.

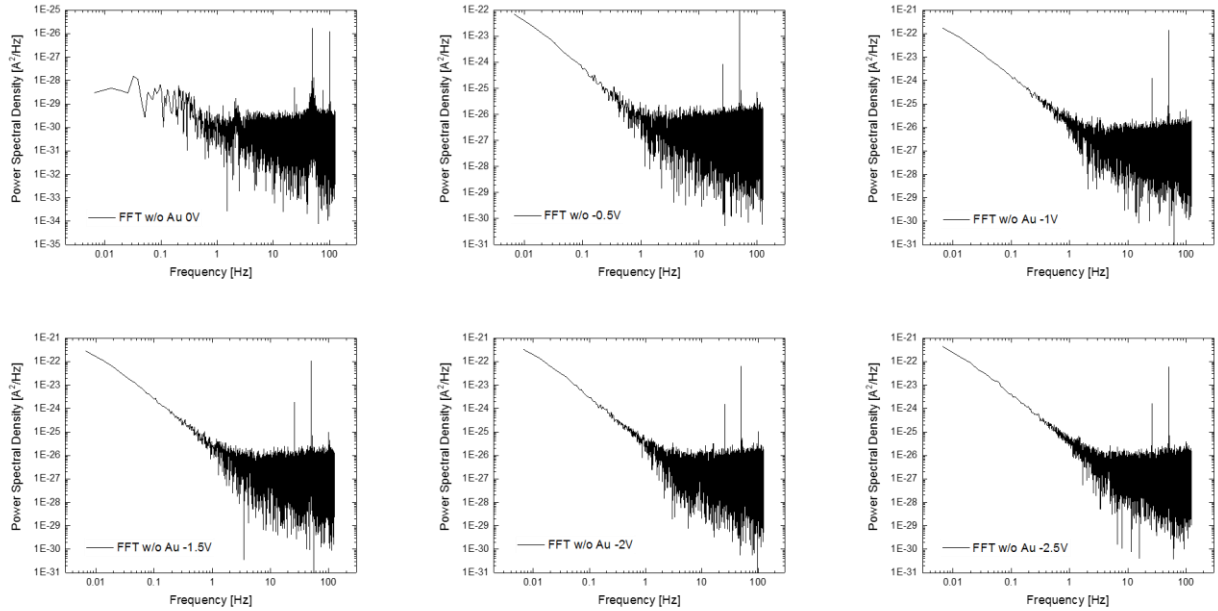

Figure S3 Noise spectral density of low-Q electrically inverted OPDs at various voltages measured at a bandwidth of 0.01 Hz (100 second time constant). These results were obtained by applying a fast Fourier transform on the current versus time measured up to 200s with intervals of 4 ms.

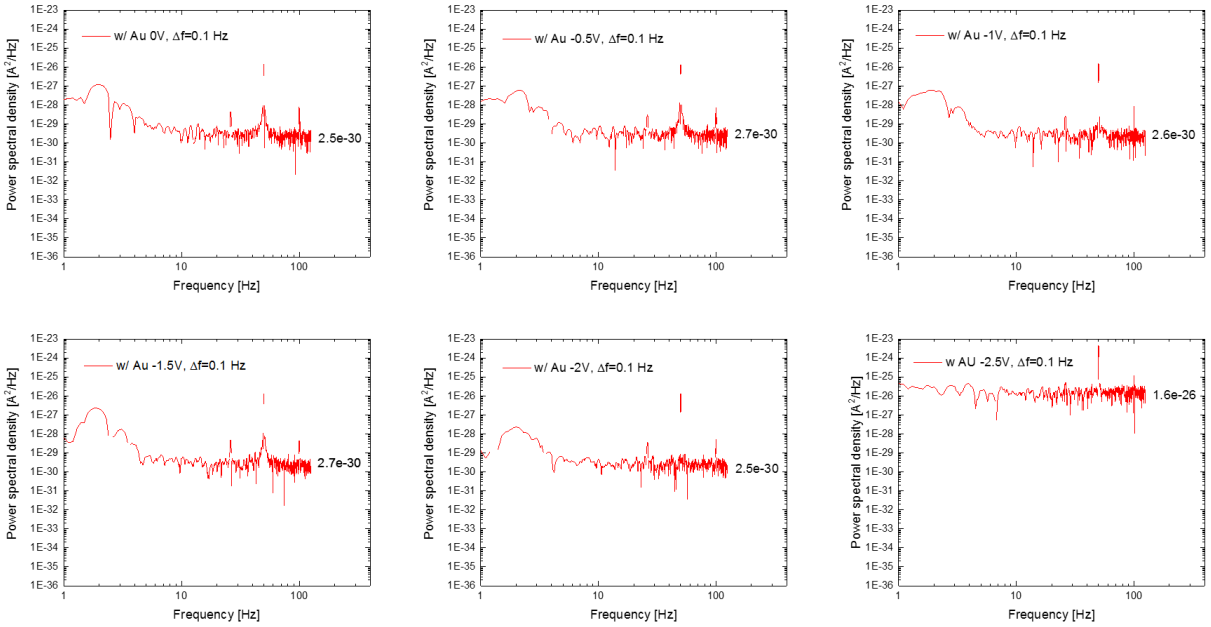

Figure S4 Noise spectral density of high-Q electrically inverted OPDs at various voltages measured at a bandwidth of 0.1 Hz (10 second time constant). These results were obtained by applying a fast Fourier transform on the current versus time measured up to 200s with intervals of 4 ms.

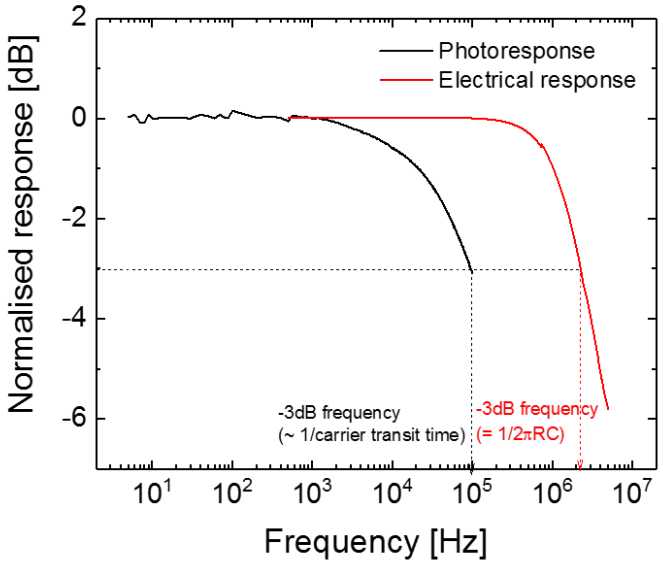

Figure S5 Electrically inverted OPD Frequency bandwidth. The normalised response of the photodetector with junction thickness of 700 nm measured with a fast LED driven by a network analyser (off-diagonal scattering matrix). The -3dB cut-off frequency is 100 kHz. The red curve shows the electrical response of the device in reverse bias (also measured with a network analyser in reflection mode) indicating an RC-limited frequency bandwidth of 2 MHz. The cut-off frequency of the device is therefore limited by the transit time of the charge carriers and not the RC-time.